Fokker-Planck description of conductance-based integrate-and-fire neuronal networks

Gregor Kovačič,[1] Louis Tao,[2] Aaditya V. Rangan,[3] and David Cai[3,4,*]

[1]*Department of Mathematical Sciences, Rensselaer Polytechnic Institute, 110 8th Street, Troy, New York 12180, USA*

[2]*Center for Bioinformatics, National Laboratory of Protein Engineering and Plant Genetics Engineering, College of Life Sciences, Peking University, 5 Summer Palace Road, Beijing 100871, People's Republic of China*

[3]*Courant Institute of Mathematical Sciences, New York University, 251 Mercer Street, New York, New York 10012-1185, USA*

[4]*Department of Mathematics, Shanghai Jiao Tong University, Dong Chuan Road 800, Shanghai 200240, People's Republic of China*

(Received 3 April 2009; revised manuscript received 27 June 2009; published 6 August 2009)

Steady dynamics of coupled conductance-based integrate-and-fire neuronal networks in the limit of small fluctuations is studied via the equilibrium states of a Fokker-Planck equation. An asymptotic approximation for the membrane-potential probability density function is derived and the corresponding gain curves are found. Validity conditions are discussed for the Fokker-Planck description and verified via direct numerical simulations.

DOI: 10.1103/PhysRevE.80.021904 PACS number(s): 87.19.L−, 05.20.Dd, 84.35.+i

I. INTRODUCTION

The use of kinetic theory for describing many-body interactions has a long tradition reaching back at least to the work of Boltzmann [1,2]. Before the advent of direct numerical simulations made possible by powerful computers, this and related coarse-grained statistical theories generally provided the only practical means for addressing large-scale problems. Only recently have direct numerical simulations of large assemblies of individual particles, waves, or neurons advanced to the degree that they provide qualitatively if not quantitatively accurate descriptions of the problems under study. Two examples of the use of kinetic theory for objects other than particles are wave turbulence [3–9] and neuroscience [10,11]. Subsequent simulations of turbulent wave dynamics [12–17] and neuronal processing in parts of the cerebral cortex [18–26] largely confirmed the predictions obtained via the kinetic theory. Even now, important roles remain for the kinetic and like theories, both in finding solutions to problems that are still too large to be amenable to simulation and also in identifying and providing a more fundamental understanding of mechanisms underlying physical phenomena under study. It is therefore important to study analytically the mathematical properties of these coarse-grained theories.

In this work, we study the basic properties of the kinetic theory for the simplest version of conductance-driven integrate-and-fire (IF) models of all-to-all coupled excitatory neuronal networks. In this version, we use the approximation that, upon receiving a spike, the excitatory conductances both rise and decay infinitely fast. After the introduction of the diffusion approximation in the limit of small synaptic-input fluctuations, the kinetic theory reduces to a Fokker-Planck equation for the probability density function of the neuronal membrane potential in the network [27,28]. Extensive studies of this equation for a *feed-forward* neuron driven by white and colored noise were performed in [29–34]. Here, we investigate several important theoretical consequences of the Fokker-Planck equation for an all-to-all coupled *network* of neurons. In particular, we analyze the asymptotic properties of its steady-state solutions in the diffusion limit and derive from these solutions the network gain curves, i.e., curves depicting the dependence of the network firing rate on the intensity of the external driving. We find these gain curves to exhibit bistability and hysteresis for sufficiently small synaptic-input fluctuations. In addition, in the two regimes separated by the instability region, we derive explicit asymptotic solutions of the Fokker-Planck equation describing the voltage probability density function, and also segments of the gain curves, in terms of elementary functions. We emphasize that the problem involving the Fokker-Planck equation which we study here is not of the usual linear type. Instead, it is highly nonlinear due to the presence of the average neuronal firing rate as a multiplicative self-consistency parameter in both the equation and its boundary conditions. This presence is due to the fact that the Fokker-Planck equation in this case describes statistically the dynamics of an entire neuronal network, not just a single neuron.

Typically, two types of coarse-grained descriptions are considered for neuronal networks: mean-driven [10,35–39] and fluctuation-driven [11,28,40–56]. The former only accurately describes the network activity when the mean of the external drive is by itself strong enough to induce neuronal spiking, while the latter is also valid in the regime in which considering the mean of the external drive alone would predict no spiking at all. In the limit of vanishing synaptic-input fluctuations, the kinetic theory studied in this work reproduces a version of the mean-driven model of [38] and we show how this model can be solved exactly by an explicit parametrization. We provide a complete description of this mean-driven model's gain curves, including their bistability intervals and asymptotic behavior for large values of external drive. We also investigate how the solutions and gain curves obtained from the Fokker-Planck equation approach the corresponding mean-driven solutions and gain curves in the limit as the synaptic-input fluctuations decrease and eventually vanish.

Finally, we study the validity of the Fokker-Planck description by comparison to direct numerical simulations of a conductance-based IF neuronal network with very short con-

*Email: cai@cims.nyu.edu

ductance rise and decay times. In the regime of small synaptic-input fluctuations, in which the Fokker-Planck equation is expected to be valid, we indeed find excellent agreement between the simulations and theory. When the ratio of the synaptic-input fluctuations to its mean exceeds the values for which the Fokker-Planck description is appropriate, we find that the theoretical gain curves still have a functional form very similar to that of the curves obtained through simulations, except that their slopes at high drive values become too large.

The remainder of this paper is organized as follows. In Sec. II, we describe the IF model under investigation. In Sec. III, we present the kinetic equation derived from this IF model and discuss how to obtain the network firing rate from it. In Sec. IV, we introduce the diffusion approximation and derive the corresponding Fokker-Planck equation from the kinetic equation in the diffusion limit. We also describe the validity conditions for the diffusion limit in terms of the original IF network properties. In Sec. V, we give a complete analytical solution of the mean-driven limit and find its bistability intervals. The exact solution for the voltage probability density function in terms of integrals is described in Sec. VI and an exact equation for the corresponding gain curve is derived in terms of generalized hypergeometric functions. In Sec. VII, we present a uniform asymptotic approximation for the voltage probability density function valid in the regime of small synaptic-input fluctuations and use it to find the functional form of the gain curves. In Sec. VIII, we find two simpler asymptotic approximations for this density function and the gain curves away from the bistability region. The validity of the Fokker-Planck description is discussed via comparison to direct numerical simulations of an IF network with short conductance rise and decay times in Sec. IX. Implications and ramifications of the results are discussed in Sec. X. Finally, in the Appendix, a detailed derivation of the uniform asymptotic approximation for the voltage probability density function for small synaptic-input fluctuations is described.

II. INTEGRATE-AND-FIRE NETWORK

We consider a conductance-based IF neuronal network composed of N excitatory neurons with instantaneous conductance rise and decay rates [57]. The dynamics of the membrane potential V_i of the ith neuron in this network is described by the linear differential equation

$$\tau\frac{dV_i}{dt} = -(V_i-\varepsilon_r) - \left[f\sum_j \delta(t-\tau_{ij}) + \frac{S}{pN}\sum_{\substack{k=1\\k\neq i}}^{N}\sum_l p_{ikl}\delta(t-t_{kl})\right] \times (V_i-\varepsilon_E). \tag{1}$$

Here, the expression in the square brackets describes the ith neuron's conductance arising from its synaptic input. The first term of this expression represents the contribution from the afferent external input spikes and the second from the network spikes. Among the parameters in Eq. (1), τ is the leakage time scale, τ_{ij} is the jth spike time of the external input to the ith neuron, t_{kl} is the lth spike time of the kth neuron in the network, f is the external input spike strength, S/pN is the coupling strength, ε_r is the reset potential, and ε_E is the excitatory reversal potential. We assume the nondimensionalized values

$$\varepsilon_r = 0, \quad V_T = 1, \quad \varepsilon_E = \frac{14}{3}, \tag{2}$$

with V_T being the firing threshold. For the leakage time scale, we assume $\tau=20$ ms, which corresponds to $\tau=1$ in our dimensionless units. The coefficients p_{ikl} model the stochastic nature of the synaptic release [58–63]. Each of them is an independent Bernoulli-distributed random variable such that $p_{ikl}=1$ with probability p and 0 with probability $1-p$ at the time t_{kl} when a network spike arrives at the ith neuron. We scale the coupling strength by the "effective size" of the network, pN, so that the total network input to each neuron remains finite in the limit of large network size N and does not vanish for small values of the synaptic release probability p.

Except at the spike times τ_{ij} or t_{kl}, the membrane potential V_i decays exponentially toward the reset potential ε_r, as indicated by the first term on the right-hand side of Eq. (1). When the ith neuron receives a spike, its membrane potential jumps. The relation between the values of the ith neuron's membrane potential V_i immediately before and after the times of its incoming spikes is derived to be

$$V_i(\tau_{ij}^+) = (1-\Gamma)V_i(\tau_{ij}^-) + \Gamma\varepsilon_E, \quad \Gamma = 1-e^{-f/\tau} \tag{3a}$$

for an external input spike and

$$V_i(t_{kl}^+) = (1-\Sigma)V_i(t_{kl}^-) + \Sigma\varepsilon_E, \quad \Sigma = 1-e^{-S/pN\tau} \tag{3b}$$

for a network neuron spike, provided $V_i(\tau_{ij}^+)$, $V_i(t_{kl}^+)<V_T$, respectively [28,55]. Here, the superscripts + and − denote the right-hand and left-hand limits, respectively.

Since in the absence of incoming spikes, its voltage can only decrease, any neuron in the network (1) can only spike when it receives a spike itself. In particular, the kth neuron can only spike when its membrane potential exceeds the firing threshold V_T as a result of a jump in Eq. (3a) or one or more simultaneous jumps in Eq. (3b). At this time, say t_{kl}, a spike is distributed to each of the other neurons in the network, i.e., the term $(S/pN)\delta(t-t_{kl})(V_i-\varepsilon_E)$ is added with probability p_{ikl} to every equation for the membrane potential (1) with $i=1,\ldots,N$, $i\neq k$. The kth neuron's membrane potential V_k is reset to the value ε_r. Note that every membrane potential V_i remains confined in the interval $\varepsilon_r\leq V_i\leq V_T$ for all times.

We assume that the external input spike train $\{\tau_{ij}\}$ arriving at the ith neuron in the network is an independent Poisson process for every $i=1,\ldots,N$, with the rate $\nu(t)$. The spikings of any given network neuron do not, in general, constitute a Poisson process. Moreover, as described in the previous paragraph, each of the ith neuron's spike times must coincide either with a spike time of its external drive or a spike time of one or more other network neurons, which again coincides with a spike time of some network neuron's external drive. However, we are mainly interested in the case of high external-drive Poisson rate, $\nu(t)\gg 1/\tau$, and moderate

population-averaged firing rate per neuron, $m(t)$. (This implies that the external-drive spike strength f should be small.) Thus, if the number of neurons N in the network is sufficiently large and the synaptic release probability p sufficiently small, we can assume that each neuron spikes approximately independently of other network neurons and of its own external drive and also relatively infrequently. Therefore, we are justified in assuming that the network spike times, $\{t_{kl}|k=1,\ldots,N,\ l=1,2,\ldots\}$, can be approximated by a Poisson process [64] and that this process is approximately independent of the external-drive spike trains to the network neurons. Note that the network firing rate is $Nm(t)$, where $m(t)$ is the population-averaged firing rate per neuron in the network referred to above.

III. KINETIC EQUATION

A probabilistic description of the network dynamics for Eq. (1) is obtained by considering the probability density

$$\rho(v,t) = \frac{1}{N}\sum_{i=1}^{N} \mathbb{E}\{\delta[v - V_i(t)]\}, \tag{4}$$

where $\mathbb{E}(\cdot)$ is the expectation over all realizations of the external input spike trains and all initial conditions. The kinetic equation for $\rho(v,t)$,

$$\begin{aligned}\partial_t \rho(v,t) = \partial_v\left[\left(\frac{v-\varepsilon_r}{\tau}\right)\rho(v,t)\right] + \nu(t)\left[\frac{1}{1-\Gamma}\rho\left(\frac{v-\Gamma\varepsilon_E}{1-\Gamma},t\right)\right.\\ \left. - \rho(v,t)\right] + Npm(t)\left[\frac{1}{1-\Sigma}\rho\left(\frac{v-\Sigma\varepsilon_E}{1-\Sigma},t\right) - \rho(v,t)\right]\\ + m(t)\delta(v-\varepsilon_r),\end{aligned} \tag{5}$$

is derived in a way similar to [28,55], where the coefficients Γ and Σ are as in Eqs. (3a) and (3b). The last term in Eq. (5) represents the probability source due to the neuronal membrane potentials being reset to $v=\varepsilon_r$ after crossing the firing threshold at $v=V_T$.

Equation (5) can be written in the conservation form

$$\partial_t \rho(v,t) + \partial_v J(v,t) = m(t)\delta(v-\varepsilon_r), \tag{6}$$

with the probability flux

$$J(v,t) = J_S(v,t) + J_I(v,t). \tag{7}$$

Here,

$$J_S(v,t) = -\left(\frac{v-\varepsilon_r}{\tau}\right)\rho(v,t) \tag{8a}$$

is the flux due to the smooth streaming of phase points under the relaxation dynamics in Eq. (1), while

$$\begin{aligned}J_I(v,t) = \nu(t)\int_{(v-\Gamma\varepsilon_E)/(1-\Gamma)}^{v} \rho(u,t)du\\ + Npm(t)\int_{(v-\Sigma\varepsilon_E)/(1-\Sigma)}^{v} \rho(u,t)du\end{aligned} \tag{8b}$$

is the flux due to jumps induced by both the external input and neuronal spiking.

A boundary condition for Eq. (5) can be derived by recalling that a neuron in the network (1) can only fire upon receiving a spike and that its membrane potential cannot stream up to move across the firing threshold V_T. Thus, on the one hand,

$$J_S(V_T,t) = -\left(\frac{V_T-\varepsilon_r}{\tau}\right)\rho(V_T,t) \le 0,$$

but on the other hand, negative relaxation flux at $v=V_T$ is impossible since no neuron's voltage can ever stream back down from V_T via relaxation: once it reaches the threshold V_T, it can only return to the reset value ε_r. Therefore,

$$J_S(V_T,t) \equiv 0 \tag{9}$$

and so

$$\rho(V_T,t) \equiv 0 \tag{10}$$

is a boundary condition for Eq. (5) [28,55].

The firing rate $m(t)$ is given by the probability flux $J(V_T,t)$ across the threshold V_T, which, in light of the definitions (7) and (8b) and the boundary condition (9), reads

$$\begin{aligned}m(t) = J(V_T,t) = J_I(V_T,t) = \nu(t)\int_{(V_T-\Gamma\varepsilon_E)/(1-\Gamma)}^{V_T} \rho(u,t)du\\ + Npm(t)\int_{(V_T-\Sigma\varepsilon_E)/(1-\Sigma)}^{V_T} \rho(u,t)du.\end{aligned} \tag{11}$$

Moreover, since $\rho(v,t)$ is a probability density function defined on the v interval $\varepsilon_r < v < V_T$, it must satisfy the nonnegativity condition

$$\rho(v,t) \ge 0 \tag{12}$$

and the normalization condition

$$\int_{\varepsilon_r}^{V_T} \rho(v,t)dv = 1. \tag{13}$$

The simultaneous presence of the firing rate $m(t)$ as a self-consistency parameter in the kinetic equation (5) and the boundary conditions (11), together with the normalization condition (13), makes the problem at hand highly nonlinear.

IV. FOKKER-PLANCK EQUATION

For small values of the external drive and network spike strengths, f and S/pN, respectively, we can obtain the diffusion approximation to the kinetic Eq. (5) by Taylor-expanding the differences in the terms arising from the voltage jumps [55]. Here, the smallness of the spike strengths f and S/pN is interpreted in terms of the minimal number of spike-induced voltage jumps a neuron with the initial membrane potential at the reset value ε_r must undergo in order to fire. In particular, this number must be large for the diffusion approximation to hold. Using the jump conditions (3a) and (3b), this requirement gives rise to the jump-size estimates

$$f, \frac{S}{pN} \ll \tau\frac{B-1}{B}, \tag{14}$$

where

$$B = \frac{\varepsilon_E - \varepsilon_r}{\varepsilon_E - V_T}. \tag{15}$$

The number of jumps can be estimated by the smaller of the two ratios, $[\tau(B-1)/B]/f$ or $[\tau(B-1)/B]/(S/pN)$. Moreover, in this regime, in order for the network neurons to maintain nonvanishing firing rates, the input Poisson rate must be sufficiently large. In particular, the external input spike strength f and the Poisson rate ν must satisfy the conditions

$$\frac{f}{\tau} \ll 1, \quad \nu\tau \gg 1, \quad f\nu = O(1). \tag{16}$$

Note that these conditions are consistent with the requirement that the spike train produced jointly by the network neurons be (approximately) independent of any individual neuron's external driving train, discussed at the end of Sec. II.

An equivalent approach to Taylor-expanding the difference terms in Eq. (5) is to approximate Eq. (6) by expanding the probability flux $J(v,t)$ in Eq. (7) using the trapezoidal rule to evaluate the respective integrals in Eq. (8b). Thus, we obtain for Eq. (7) the expression

$$J(v,t) = -\frac{1}{\tau}\{[(a+q^2)v - (a+q^2-1)\varepsilon_E - \varepsilon_r]\rho(v,t) + q^2(\varepsilon_E - v)^2\partial_v\rho(v,t)\}, \tag{17}$$

with the coefficients

$$a = 1 + f\nu + Sm, \quad q^2 = \frac{1}{2\tau}\left(f^2\nu + \frac{S^2 m}{pN}\right). \tag{18}$$

The flux (7) satisfies the equation

$$J(\varepsilon_r^+) - J(\varepsilon_r^-) = m(t),$$

as can be gleaned from Eq. (6). Moreover, since $\rho(v < \varepsilon_r, t) \equiv 0$, we have $J(v < \varepsilon_r, t) \equiv 0$ and we find that for $\varepsilon_r < v < V_T$ the probability density function $\rho(v,t)$ obeys the partial differential equation

$$\partial_t\rho(v,t) + \partial_v J(v,t) = 0, \tag{19}$$

that is, the Fokker-Planck equation

$$\tau\partial_t\rho(v,t) = \partial_v\{[(a+q^2)v - (a+q^2-1)\varepsilon_E - \varepsilon_r]\rho(v,t) + q^2(\varepsilon_E - v)^2\partial_v\rho(v,t)\}, \tag{20}$$

with the flux boundary condition

$$J(\varepsilon_r^+, t) = J(V_T, t) = m(t). \tag{21}$$

Here, the flux $J(v,t)$ is given by Eq. (17) [28,54,55].

We retain the boundary condition $\rho(V_T,t)=0$ in Eq. (10) as the absorbing boundary condition for the Fokker-Planck equation (20) in the diffusion limit [28,55]. Likewise, we retain the non-negativity condition (12) and the normalization condition (13). In this approximation, again, the Fokker-Planck equation (20), together with the boundary conditions (10) and (21) and the normalization condition (13), gives rise to a highly nonlinear problem due to the simultaneous occurrence of the firing rate $m(t)$ as a multiplicative self-consistency parameter in both Eqs. (20) and (21).

Note that the ratio q^2/a of the two coefficients a and q^2, as defined in Eq. (18), is controlled by the two jump sizes, f/τ and $S/\tau pN$, which also control the validity of the diffusion approximation according to Eq. (14). Since the ratio q^2/a controls the size of the fluctuation term in Eq. (20), the inequalities in Eqs. (14) and (16) imply that the diffusion approximation leading to the Fokker-Planck equation (20) also prompts the corresponding neuronal dynamics to be in the small-fluctuation limit

$$\frac{q^2}{a} \ll 1. \tag{22}$$

We will be primarily interested in the steady solutions of Eq. (20). In view of the conservation form (19), with $J(v,t)$ as in Eq. (17) and the boundary conditions (21), we find that Eq. (20) can in this case be replaced by the first-order linear differential equation

$$[(a+q^2)v - (a+q^2-1)\varepsilon_E - \varepsilon_r]\rho(v) + q^2(\varepsilon_E - v)^2\partial_v\rho(v) = -m\tau, \tag{23}$$

with a and q defined in Eq. (18). We require the steady probability density function $\rho(v)$ to satisfy the boundary condition $\rho(V_T)=0$ in Eq. (10), as well as the conditions (12) and (13). From these equations, we can derive the gain curve, i.e., the firing rate m as a function of the external driving strength $f\nu$. We carry out this derivation and its analysis below.

V. MEAN-DRIVEN AND FLUCTUATION-DRIVEN LIMITS

We begin by analyzing the limiting case of the regime in Eq. (16) in which $f \to 0$ and pN, $\nu \to \infty$ such that $f\nu = O(1)$. There are no input conductance fluctuations in this limit and so $q^2/a \to 0$ in Eq. (22). Note that, in this limit, the effect of the external-drive Poisson train on the network dynamics becomes identical to that of a time-independent excitatory conductance with the mean value of this train's strength, $f\nu$.

The stationary equation (23) in this limit reduces to

$$\rho(v) = \frac{\tau m}{a(V_S - v)}, \tag{24}$$

where

$$V_S = \frac{\varepsilon_r + (a-1)\varepsilon_E}{a} \tag{25}$$

is the effective reversal potential [65] and a is defined in Eq. (18). Since the v derivative $\partial_v\rho(v)$ in Eq. (23) is lost in the limit as $q \to 0$, it is consistent to naturally drop the boundary condition (10).

The density $\rho(v)$ in Eq. (24) must satisfy the condition $\rho(v) \geq 0$ in Eq. (12) for $\varepsilon_r \leq v \leq V_T$. Since $a > 0$, it is easy to show that $V_S > \varepsilon_r$ and so the condition (12) is satisfied when

$$V_T < V_S, \quad \text{i.e.,} \quad a > B, \tag{26}$$

where B is defined as in Eq. (15). The condition $a > B$ corresponds to the fact that the neuronal voltages must stream

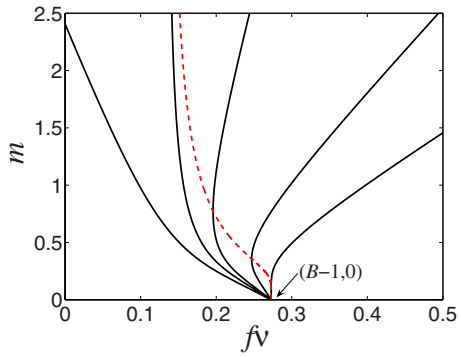

FIG. 1. (Color online) Black: gain curves m as a function of $f\nu$ in the mean-driven limit. Gray (red online) dashed line: the locations of the saddle-node bifurcation points on the gain curves. The parameter values are $B=14/11=1.2727$, and $\tau=1$. The reversal and threshold potentials satisfy Eq. (2). The coupling strengths along the gain curves are (left to right) $S=0.3$, $S=\tau \ln B=0.2412$, $S=0.2$, $S=0.1$, and $S=0$.

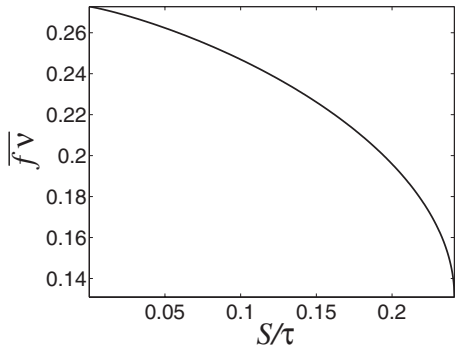

FIG. 2. The $f\nu$ coordinate, $\overline{f\nu}$, of the firing-rate saddle-node bifurcation as a function of S/τ. The parameter values are $B=14/11=1.2727$ and $\tau=1$. The reversal and threshold potentials satisfy Eqs. (2).

upwards at the threshold V_T for the neurons to fire; in other words, $m\neq 0$ under the mean drive $f\nu+Sm$. The normalization condition (13) then yields

$$m=\frac{a}{\tau \ln\frac{V_S-\varepsilon_r}{V_S-V_T}}. \tag{27}$$

From Eqs. (18) and (25), we observe that Eq. (27) gives a nonlinear equation for the firing rate m in terms of the driving strength $f\nu$. In view of the comment made in the first paragraph of this section that the neuronal dynamics in the present limit are driven by the mean of the external input spike train, we refer to Eq. (27) as describing the *mean-driven limit* of our neuronal network.

The case when $V_S<V_T$, i.e., $a<B$, corresponds to the case when $m=0$. Replacing the external drive in Eq. (1) by its mean $f\nu$, we find that all the neuronal membrane potentials settle at the value $v=V_S$ after a time period of $O(\tau)$ and this is why no neurons can spike. In other words, the steady-state voltage probability density $\rho(v)$ becomes $\rho(v)=\delta(v-V_S)$, where $\delta(\cdot)$ is again the Dirac delta function. This result can also be deduced from the appropriate solution to the full Eq. (23), as will be done in Sec. VIII A. We will refer to the corresponding operating regime of the network, depicted by the interval $0<f\nu<B-1$ in the $f\nu-m$ plane shown in Fig. 1, as the *fluctuation-driven* regime. In particular, in the present limit of vanishing fluctuations, the network firing rate also vanishes in this regime.

We now return to analyzing the solution of Eq. (27). From Eqs. (15), (18), (25), and (27), we arrive at the *exact parametric representation* of the $m-f\nu$ gain curve in terms of the parameter a,

$$m=\frac{a}{\tau \ln\frac{B(a-1)}{a-B}}, \tag{28a}$$

$$f\nu=a-1-\frac{Sa}{\tau \ln\frac{B(a-1)}{a-B}}, \tag{28b}$$

which holds in the *mean-driven regime*, $a>B$. In particular, for every a, we can find the exact value of the firing rate m that corresponds to its external drive $f\nu$.

The graphs of the gain curves, m versus $f\nu$, in the mean-driven limit, are presented in Fig. 1 for several different values of the parameter S. From simple analysis, it is clear that the graph of m versus $f\nu$ begins at the "driving threshold" value, $f\nu=B-1=(V_T-\varepsilon_r)/(\varepsilon_E-\varepsilon_r)$, and $m=0$, going backward in $f\nu$, with the initial derivative $-1/S$. The threshold value $f\nu=B-1$ corresponds to the external input Poisson spike rate ν being sufficiently large that, on average, the rate of the neuronal membrane-potential increase in the IF network (1) induced by the external input spikes exceeds its downward streaming rate due to the leakage.

For large values of the parameter a, every gain curve asymptotes toward its own straight line

$$m=\frac{f\nu+1-(B-1)/\ln B}{\tau \ln B-S}. \tag{29}$$

If $S>\tau \ln B$, the gain curve has a negative slope everywhere and terminates with a nonzero firing rate m at $f\nu=0$, such as the leftmost curve in Fig. 1. If $S<\tau \ln B$, the gain curve turns around in a saddle-node bifurcation, such as the second and third gain curves from the right in Fig. 1. The location of this saddle-node bifurcation is at the intersection of the gain curve and the gray (red online) dashed curve in Fig. 1. The gain curve passes through a bistability interval that begins at the saddle-node bifurcation point and ends at the driving threshold $f\nu=B-1$. The gain curve in the limit of vanishing coupling strength, $S\to 0$, has an infinite derivative at the point $f\nu=B-1$ and $m=0$ and then monotonically increases as a graph of m versus $f\nu$ with a monotonically decreasing derivative, reflecting the fact that an uncoupled neuron exhibits no bistability.

The dependence on the parameter S/τ of the driving strength $f\nu$ at the saddle-node bifurcation point, which exists for $0<S<\tau \ln B$, is displayed in Fig. 2. It is obtained as the

minimum value, $\overline{f\nu}$, of $f\nu$ in Eq. (28b), from which we also see that it is clearly a function of the ratio S/τ alone. As $S/\tau \to 0$ along this bifurcation curve, $\overline{f\nu} \to B-1$, again indicating the absence of a bistability region for an uncoupled neuron. The curve of the saddle-node bifurcation point locations in the $f\nu - m$ plane, parametrized by the coupling constant S, is shown in gray (red online) in Fig. 1.

We remark that, for the current-based version of the IF model (1), the analog of Eq. (27) can be solved explicitly for the external driving strength $f\nu$ in terms of the firing rate m [66,67]. The gain-curve shapes in the mean-driven limit for both types of models are similar.

VI. EXACT IMPLICIT SOLUTION

To address the gain curves with finite synaptic-input fluctuations as obtained from the full Eq. (23), it will be convenient to introduce the new independent variable

$$x = \frac{\varepsilon_E - \varepsilon_r}{\varepsilon_E - v}. \tag{30}$$

Note that the reset potential $v=\varepsilon_r$ here corresponds to $x=1$ and the firing threshold $v=V_T$ to $x=B$, with B as in Eq. (15).

It will also be convenient to introduce the new dependent variable $\varrho(x)$, which must satisfy the requirement $\varrho(x)dx = \rho(v)dv$. This requirement gives

$$\rho(v) = \frac{x^2 \varrho(x)}{\varepsilon_E - \varepsilon_r}, \tag{31}$$

and Eqs. (23), (30), and (31) imply that the equation for the density $\varrho(x)$ becomes

$$q^2 x^2 \varrho' + x(x + q^2 - a)\varrho = -m\tau, \tag{32}$$

where the prime denotes differentiation upon x. The boundary condition (10) becomes

$$\varrho(B) = 0 \tag{33}$$

and the normalization condition (13) becomes

$$\int_1^B \varrho(x)dx = 1, \tag{34}$$

with B as in Eq. (15).

The exact solution of Eq. (32), satisfying the conditions (33) and (34), is given by

$$\varrho(x) = \frac{m\tau}{q^2} x^{a/q^2-1} e^{-x/q^2} \int_x^B s^{-a/q^2-1} e^{s/q^2} ds. \tag{35}$$

Integrating the density (35) over the interval $1<x<B$, we find that the normalization condition (34) becomes

$$\frac{m\tau}{q^2} \int_1^B s^{-a/q^2-1} e^{s/q^2} ds \int_1^s x^{a/q^2-1} e^{-x/q^2} dx = 1, \tag{36}$$

which can be rewritten in terms of the confluent hypergeometric function ${}_1F_1$ [68] as

$$\frac{m\tau}{a}\left\{ \int_1^B \frac{1}{s} {}_1F_1\left(1, \frac{a}{q^2}+1, \frac{s}{q^2}\right) ds + \frac{q^2}{a} {}_1F_1\left(\frac{a}{q^2}, \frac{a}{q^2}+1, -\frac{1}{q^2}\right) \times \left[B^{-a/q^2} {}_1F_1\left(-\frac{a}{q^2}, -\frac{a}{q^2}+1, \frac{B}{q^2}\right) - {}_1F_1\left(-\frac{a}{q^2}, -\frac{a}{q^2}+1, \frac{1}{q^2}\right)\right]\right\} = 1. \tag{37}$$

After performing the last integration and transforming the result using known identities for (generalized) hypergeometric functions [69], we finally arrive at

$$\frac{m\tau}{a}\left\{ \ln B + \frac{1}{a+q^2}\left[B\, {}_2F_2\left([1,1], \left[2, \frac{a}{q^2}+2\right], \frac{B}{q^2}\right) - {}_2F_2\left([1,1], \left[2, \frac{a}{q^2}+2\right], \frac{1}{q^2}\right)\right] + \frac{q^2}{a} {}_1F_1\left(1, \frac{a}{q^2}+1, \frac{1}{q^2}\right) \times \left[B^{-a/q^2} e^{(B-1)/q^2} {}_1F_1\left(1, -\frac{a}{q^2}+1, -\frac{B}{q^2}\right) - {}_1F_1\left(1, -\frac{a}{q^2}+1, -\frac{1}{q^2}\right)\right]\right\} = 1. \tag{38}$$

Here, ${}_kF_l$ is the generalized hypergeometric function

$${}_kF_l([\alpha_1, \ldots, \alpha_k], [\beta_1, \ldots, \beta_l], z) = \sum_{n=0}^{\infty} \frac{(\alpha_1)_n \cdots (\alpha_k)_n}{(\beta_1)_n \cdots (\beta_l)_n} \frac{z^n}{n!},$$

with $(\gamma)_j = \gamma(\gamma+1)\cdots(\gamma+j-1)$ being the Pochhammer symbol [68].

In light of the definitions of the coefficients a and q^2 in Eq. (18), we observe that Eq. (38) gives a nonlinear equation connecting the driving $f\nu$ and the firing rate m.

VII. GAIN CURVES

Equation (38) is of little practical use in computing the gain curves due to the difficulties in evaluating hypergeometric functions of large arguments [70]. Instead, we can rewrite Eq. (36) as

$$\frac{m\tau}{q^2} \int_{1/q^2}^{B/q^2} y^{-a/q^2-1} e^y \left[\gamma\left(\frac{a}{q^2}, y\right) - \gamma\left(\frac{a}{q^2}, \frac{1}{q^2}\right)\right] dy = 1, \tag{39}$$

where $\gamma(\alpha, z) = \int_0^z t^{\alpha-1} e^{-t} dt$ is the incomplete Gamma function, and perform the integration and solve the equation in Eq. (39) numerically using the functional dependence (18) of a and q^2 on $f\nu$ and m.

Alternatively, we can recall that our investigation of the gain curves is only valid in the small-fluctuation limit (22), $q^2/a \ll 1$, of the Fokker-Planck equation (20), due to the conditions (14) and (16) imposed by the diffusion approximation. In this limit, as described in the Appendix, it follows from the result of [71] that the probability density $\varrho(x)$ in Eq. (35) has an asymptotic expansion in terms of q^2/a, uniform in x, a, and/or q, whose first two terms are given by

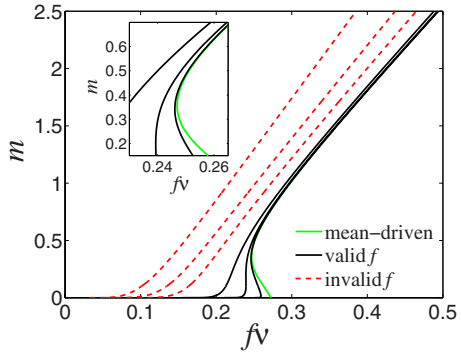

FIG. 3. (Color online) Gain curve: the firing rate m as a function of the driving strength $f\nu$. The reversal and threshold potentials satisfy Eq. (2). The parameter values are $\tau=1$, $S=0.1$, and $\lambda=1$, where $pN=\lambda/f$ and $\delta_s=0.0002$. The strength of the external input spikes f varies from curve to curve. From left, the values of f are 0.1, 0.05, 0.025, 0.005, 0.001, 0.0001, and 0, respectively. Note that, along the left three gain curves (dashed; red online), f does not satisfy the small-jumps condition (14) and the Fokker-Planck equation (20) becomes therefore progressively less valid with increasing f and with proportionally decreasing pN. The corresponding minimal numbers of jumps needed for a neuron to reach V_T beginning at ε_r, computed from Eq. (14), are ~2, 4, 8, 40, 200, and 2000, respectively. The rightmost gain curve (gray; green online) was plotted using the parametrization (28) in the mean-driven limit ($f=0$, $pN\to\infty$, $\nu\to\infty$, $f\nu$ finite). Inset: convergence of the gain curves to the mean-driven limit gain curve near the upper turning point as f decreases and pN increases proportionally.

$$\varrho(x) \sim \frac{m\tau}{xq}\left\{\exp\left(\frac{a[\eta^2(B)-\eta^2(x)]}{2q^2}\right)\left[\sqrt{\frac{2}{a}}D\left(\frac{\eta(B)}{q}\sqrt{\frac{a}{2}}\right)-\frac{q}{a\eta(B)}+\frac{q}{B-a}\right]-\left[\sqrt{\frac{2}{a}}D\left(\frac{\eta(x)}{q}\sqrt{\frac{a}{2}}\right)-\frac{q}{a\eta(x)}+\frac{q}{x-a}\right]\right\}, \tag{40}$$

where

$$\eta(x)=\mathrm{sgn}(x-a)\sqrt{2\left(\frac{x}{a}-1-\ln\frac{x}{a}\right)} \tag{41}$$

and $D(\cdot)$ denotes the Dawson integral

$$D(z)=e^{-z^2}\int_0^z e^{y^2}dy. \tag{42}$$

Using Eq. (34), we obtain the gain curves by numerically integrating the approximation (40) over the interval $1<x<B$ and using the functional dependence (18) of a and q^2 on $f\nu$ and m.

To compute numerically the gain curves, such as those presented in Fig. 3, in practice, we combine the above two numerical methods, either using Eq. (39) or (40). We switch from the former to the latter when the value of q^2/a drops below a prescribed tolerance, δ_s. [This is to ensure that the error of the asymptotic formula (40) at larger values of q^2/a does not affect the gain-curve shapes. However, formula (40) is so accurate that in all the figures presented in this work, the difference between the probability density functions and gain curves obtained by the two methods is imperceptible.] We see that for small external driving spike strength f and proportionally large effective network size pN, the gain curve closely follows its no-fluctuations counterpart from Fig. 1, except for a smoothed-out corner near the point $f\nu=B-1$, $m=0$. In particular, the small-f gain curves still exhibit bistability. As the value of the external driving spike strength f increases and the effective network size pN decreases at the same rate, i.e., the amount of fluctuations in the input to a single neuron increases, the backward-sloping portion of the gain curve inside the bistability interval steepens and the bistability interval narrows until it disappears. As $f\nu$ decreases, a gain curve eventually approaches the $f\nu$ axis exponentially fast in $f\nu$ (and f/τ), as we will further discuss in Sec. VIII A below.

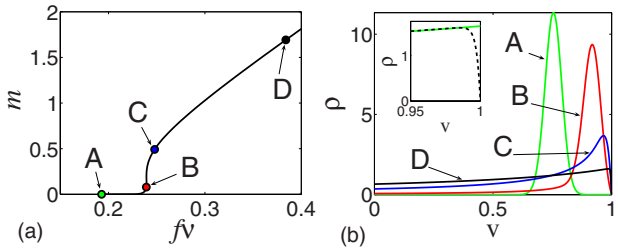

FIG. 4. (Color online) Probability density functions $\rho(v)$ at specific points on the $m-f\nu$ gain curve. The reversal and threshold potentials satisfy Eq. (2). The parameter values are $\tau=1$, $f=0.001$, $S=0.1$, $pN=1000$, and $\delta_s=0.0002$. (a) Specific points on the gain curve. (b) $\rho(v)$ at these points. The functions $\rho(v)$ were computed via the asymptotic formula (40). [Note that $\rho(v)$ computed numerically via Eqs. (30), (31), and (35) instead of Eq. (40) appear identical.] Inset: the boundary layer at $v=V_T$ of the probability density functions $\rho(v)$ corresponding to the location "D" on the high-firing part of the gain curve as shown in black dashed line. (Note the scale on the v axis.) In gray (green online) is shown $\rho(v)$ in the mean-driven limit, described by Eq. (24).

For large values of the driving $f\nu$, the gain curves in Fig. 3 increase almost linearly. In this regime, $q^2\gg 1$, the exact probability density function (35) behaves asymptotically as

$$\rho(x)\sim\frac{m\tau}{ax}\left[1-\left(\frac{x}{B}\right)^{a/q^2}\right]. \tag{43}$$

The normalization condition (34) yields the equation

$$\frac{m\tau}{a}\left[\ln B-\frac{q^2}{a}(1-B^{-a/q^2})\right]\sim 1 \tag{44}$$

for the asymptotic behavior of the gain curves, from which the slopes of the straight-line asymptotes can easily be computed. In particular, for $q^2/a\ll 1$, the limiting slope agrees with that of the straight-line asymptote in the mean-driven limit, given by Eq. (29).

On the right of Fig. 4, we present the probability density functions $\rho(v)$ corresponding to four specific points on the gain curve for $f=0.001$ in Fig. 3, which is replotted on the left of Fig. 4. The function $\rho(v)$ in the $f\nu$ regime below the

bistability interval appears very similar to a Gaussian curve, a point we will return to in Sec. VIII A. Progressing up the gain curve, the density functions undergo a shape change until the one in the $f\nu$ regime well above the bistability interval appears indistinguishable from the mean-driven-limit density $\rho(v)$ in Eq. (24), except in a thin boundary layer near $v=V_T$. In that layer, the density $\rho(v)$ in Fig. 4 decreases rapidly and vanishes at $v=V_T$ to satisfy the boundary condition (10). We will further elaborate on the gain-curve shapes in the $f\nu$ regimes above and below the bistability interval in Sec. VIII.

VIII. ASYMPTOTIC BEHAVIOR OF GAIN CURVES IN THE SMALL-FLUCTUATION LIMIT

In the small-fluctuation limit (22), i.e., for $q^2/a \ll 1$, we can derive exact asymptotic expressions for the probability density function $\rho(v)$ and the pieces of the gain curves that lie in the fluctuation-driven ($a<B$) and mean-driven ($a>B$) regimes, respectively. Roughly speaking, in Fig. 3, the former regime corresponds to the portion of the gain curve near the $f\nu$ axis and the latter to the portion near the limiting mean-driven gain curve (28), with both staying $O(q/\sqrt{a})$ away from the threshold value $f\nu=B-1$, $m=0$. The asymptotic expansions are derived using Laplace's method [72] on the integral in Eq. (35).

As we recall from Sec. V, in the fluctuation-driven regime, $a<B$, the effective reversal potential V_S in Eq. (25) lies below the firing threshold, $V_S<V_T$. The few neuronal firings that occur in this regime are driven by the membrane-potential fluctuations of individual neurons. The smallness of these fluctuations when $q^2/a \ll 1$, i.e., when f/τ, $S/\tau pN \ll 1$ in accordance with Eq. (14), leads to low firing rates. As we show in Sec. VIII A below, the neuronal firing rate m is in fact an exponentially small function of the voltage jump size f/τ.

In the mean-driven regime, $a>B$, the effective reversal potential V_S in Eq. (25) lies above the firing threshold, $V_S>V_T$. As we recall from Sec. V, due to the conditions (14) and (16), the effect of the external drive is nearly constant in time and the neuronal network firing rate is largely controlled by the mean of this drive. We now explore the asymptotic expressions for the firing rates in these two regimes in detail.

A. Fluctuation-driven regime

In the fluctuation-driven regime, $a<B$ ($V_S<V_T$), the leading order in q^2/a of the density $\varrho(x)$ is given by

$$\varrho(x) \sim \frac{m\tau}{a(B-a)} \exp\left(\frac{a\eta^2(B)}{2q^2}\right) \exp\left(-\frac{(x-a)^2}{2q^2 a}\right), \quad (45)$$

with $\eta(x)$ as in Eq. (41), which has a relative error of $O(q^2/a)$ near $x=a$ and is exponentially accurate everywhere else.

The normalization condition (34) used on Eq. (45) gives

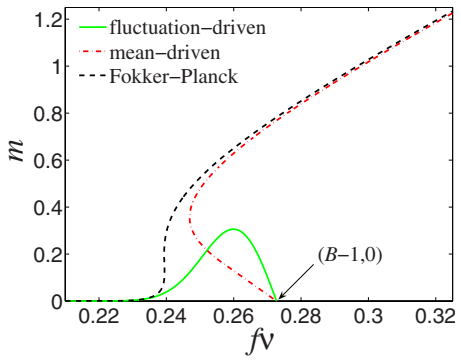

FIG. 5. (Color online) Comparison between a gain curve (black dashed) computed from the steady-state Fokker-Planck equation as described in Sec. VII (displayed on left of Fig. 4) and its approximations in the fluctuation-driven (light gray; green online) and mean-driven (dark gray dash-dotted; red online) regimes, computed via Eqs. (48) and (28), respectively. The parameter values along the computed gain curve are $\tau=1$, $f=0.001$, $S=0.1$, $pN=1000$, and $\delta_s=0.0002$. The reversal and threshold potentials satisfy Eq. (2).

$$\frac{m\tau q}{B-a} \exp\left(\frac{a\eta^2(B)}{2q^2}\right) \sqrt{\frac{\pi}{2a}} \left[1+\mathrm{erf}\left(\frac{a-1}{\sqrt{2a}q}\right)\right] \sim 1, \quad (46)$$

where $\mathrm{erf}(\cdot)$ denotes the error function $\mathrm{erf}(z)=(2/\sqrt{\pi})\int_0^z e^{-t^2}dt$.

Formula (46) implies that the firing rate m is exponentially small in q^2/a. Therefore, in this case, from Eq. (18), we find asymptotically

$$a \sim 1+f\nu, \quad q^2 \sim \frac{f^2\nu}{2\tau}. \quad (47)$$

In other words, to within an exponentially small error, the firing rate gain in this case is induced by the fluctuations in the feed-forward input to the neuron while the feed-back synaptic input from other neurons in the population is negligible. This phenomenon of "asymptotic decoupling"—i.e., under a small-fluctuation subthreshold drive, the network is asymptotically decoupled—is important for understanding small-fluctuation network dynamics.

Except when $a-1 \lesssim O(q/\sqrt{a})$, the leading order of the bracketed term containing the error function in formula (46) equals 2. From this, the assumption $f \ll 1$ and the fact that the firing rate m is exponentially small in q^2/a (and so in f) in this regime—and therefore Eq. (47) holds—we find for m the explicit leading-order approximation

$$m \sim [B-(1+f\nu)]\sqrt{\frac{1+f\nu}{\pi\tau f^2\nu}} \times \exp\left\{\frac{2\tau}{f^2\nu}\left[(1+f\nu)\left(1+\ln\frac{B}{1+f\nu}\right)-B\right]\right\}. \quad (48)$$

We remark that Eq. (48) is not valid *uniformly* in the $f\nu$ interval between 0 and $B-1$. In particular, near $f\nu=B-1$, the right-hand side of Eq. (48) becomes of size $O(1)$, contradicting the exponential smallness of the firing rate m, and so Eq. (48) ceases to be valid there, as can be seen from Fig. 5. This right-hand side has a maximum at

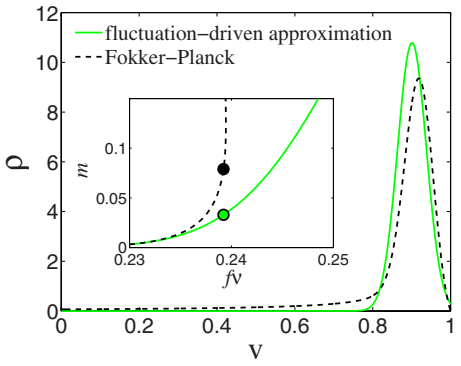

FIG. 6. (Color online) Comparison between the probability density function $\rho(v)$ computed using the uniform asymptotic approximation (40) of the steady Fokker-Planck solution and the Gaussian approximation (49), which is valid in the fluctuation-driven regime. The parameter values are $\tau=1$, $f=0.001$, $S=0.1$, and $pN=1000$. The reversal and threshold potentials satisfy Eq. (2). Inset: the value of the external driving strength $f\nu$ is the same as at the location "B" on the left panel of Fig. 4.

$$f\nu = B - 1 - \sqrt{\frac{fB(B-1)}{2\tau}} + O(f)$$

and then vanishes at $f\nu=B-1$. The location of this maximum indicates that the size of the excluded region is $O(\sqrt{f})$.

From Eqs. (30) and (47), it is clear that the probability density function $\rho(v)$ corresponding to the density $\varrho(x)$ in Eq. (45) is also Gaussian, given by the expression

$$\rho(v) \sim \sqrt{\frac{\tau(1+f\nu)^3}{\pi f^2 \nu}} \exp\left(-\frac{\tau(1+f\nu)^3(v-V_S)^2}{f^2\nu}\right), \quad (49)$$

with

$$V_S \sim \frac{\varepsilon_r + f\nu\varepsilon_E}{1+f\nu} \quad (50)$$

by Eq. (25).

In Fig. 5, we present a comparison between the approximate gain curve computed from Eq. (48) and the gain curve displayed on left of Fig. 4. The approximate gain curve follows the uniformly valid gain curve (black dashed line) very closely in the entire fluctuation-driven regime, to the point of indicating the location of the latter curve's bottom turning point shortly after the validity of Eq. (48) breaks down. Moreover, Eq. (49) provides an excellent approximation for the probability density function $\rho(v)$, as calculated via Eq. (40), throughout the fluctuation-driven regime. In particular, the curve $\rho(v)$ corresponding to the location "A" in Fig. 4 cannot be distinguished from its approximation by Eq. (49). (Data not shown.) For the curve in Fig. 4 corresponding to the location "B," which is very close to the bottom turning point of the gain curve, this Gaussian approximation still remains satisfactory, as shown in Fig. 6, even this close to the turning point.

We now also remark that Eq. (48), with an additional factor of 1/2 on the right-hand side, describes the gain-curve shape for $f\nu \ll 1$, regardless of the value of the external driving spike strength f. This is because the argument in the error function in Eq. (46) becomes $O(\sqrt{f\nu})$ and so the leading order of the bracketed term containing the error function in Eq. (46) now equals 1 rather than 2 as in Eq. (48).

Finally, we again comment on the $f\to 0$ limit in the fluctuation-driven regime, $a<B$ or $V_S<V_T$. This argument complements the argument made in Sec. V. In particular, Eq. (48) and the discussion in the paragraph following it imply that $m\to 0$ as $f\to 0$ in the entire interval $0<f\nu<B-1$. Moreover, Eq. (45), together with the normalization condition (34), implies that $\varrho(x)\to\delta(x-a)$ and so indeed $\rho(v)\to\delta(v-V_S)$, where $\delta(\cdot)$ again represents the Dirac delta function, as was mentioned in Sec. V. This argument reaffirms the observation that in the absence of input conductance fluctuations, if $V_S<V_T$, in the steady state, the external input makes all the neuronal membrane potentials equilibrate at $v=V_S$ and so no neurons can fire, as consistent with intuition.

B. Mean-driven regime

In the mean-driven regime, when $a>B$ $(V_S>V_T)$, again using a Laplace-type asymptotic expansion [72] of the integral in Eq. (35), we obtain the leading-order term in q^2/a of the density $\varrho(x)$ as

$$\varrho(x) \sim \frac{m\tau}{x(a-x)}\left\{1-\exp\left[-\frac{1}{q^2}\left(\frac{a}{B}-1\right)(B-x)\right]\right\}.$$

This equation corresponds to the probability density function

$$\rho(v) \sim \frac{m\tau}{a(V_S-v)}\left[1-\exp\left(-\frac{(a-B)(V_T-v)}{q^2(\varepsilon_E-V_T)}\right)\right] \quad (51)$$

of the original voltage variable v. This expression is equivalent to Eq. (24), except in an $O(q^2/a)$ thin boundary layer near the firing threshold $v=V_T$. This layer ensures that the boundary condition (33) is satisfied. We recall that such behavior was already observed in Fig. 4. At $O(1)$, the normalization condition (34) again yields for the firing rate m the logarithmic equation (27), whose solution via the parametrization (28) was discussed in Sec. V.

In Fig. 5, a comparison is shown between the gain curve presented on left of Fig. 4 and its approximation in the mean-driven limit obtained via Eqs. (28) for the external driving spike strength $f=0.001$. We see that the approximation is excellent deep into the mean-driven regime, but that it gradually breaks down upon approaching the bistability region in which it is invalid. For the external driving value $f\nu$ corresponding to the location "D" on the gain curve in Fig. 4, the probability density function $\rho(v)$ computed via Eqs. (28) and (51) is indistinguishable from that computed via the uniform asymptotic approximation (40). (Data not shown.) The latter is the curve "D" on the right of Fig. 4, whose boundary-layer detail is presented in the inset in Fig. 4. In Fig. 7, we display the comparison between the probability density function $\rho(v)$ corresponding to the location "C" on the left of Fig. 4 and its approximation given by Eq. (40), computed at the same value of the driving $f\nu$. The agreement still remains satisfactory, but notice that $\rho(v)$ computed from Eq. (40) has a smaller area. This is an artifact of the exponential boundary-

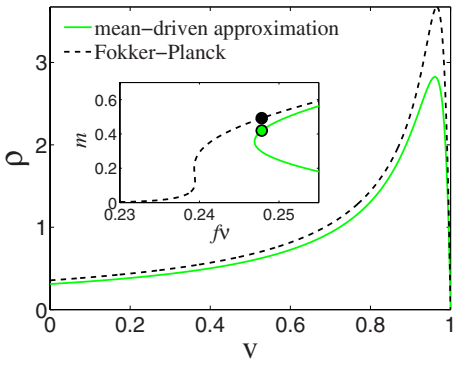

FIG. 7. (Color online) Comparison between the probability density function $\rho(v)$ computed using the uniform asymptotic approximation (40) of the steady Fokker-Planck solution and the approximation (51), which is valid in the mean-driven regime. The reversal and threshold potentials satisfy Eq. (2). The parameter values are $\tau=1$, $f=0.001$, $S=0.1$, and $pN=1000$. Note that the mean-driven approximation curve is only normalized to $O(1)$ and is missing an $O(q^2/a)$ amount, as explained in the text. Inset: the value of the external driving $f\nu$ is the same as at the location "C" on the left panel of Fig. 4.

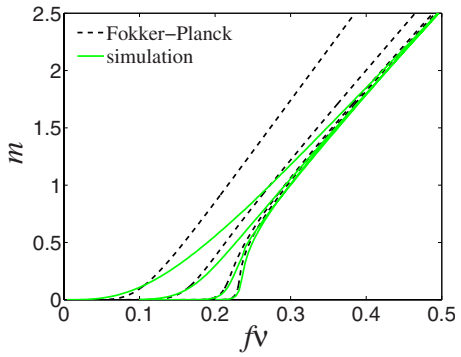

FIG. 8. (Color online) Comparison of gain curves evaluated theoretically (black, dashed) as in Sec. VII and shown in Fig. 3 and gain curves computed via numerical simulations (gray; green online). The reversal and threshold potentials satisfy Eq. (2). The parameter values are $\tau=1$, $S=0.1$, $\lambda=1$, where $pN=\lambda/f$. The strength of the external input f assumes the values 0.1, 0.025, 0.005, and 0.002, respectively, on the gain curves from left to right. In the simulations, $N=10^4$, except on the bottom half of the gain curve corresponding to $f=0.002$, where $N=2\times10^4$. The synaptic release probability p is calculated to yield the appropriate "effective network size" pN. Poisson-distributed random delays were used in computing the gain curve for $f=0.002$; the average delay was 6 ms on the bottom half and 4 ms on the top half of the gain curve. Note that, for large values of the external driving strength $f\nu$, the gain curves computed numerically appear to all asymptote toward the straight line given by Eq. (29), which is the asymptote of the gain curve (28) in the mean-driven limit for the same values of τ and S.

layer term in Eq. (40) subtracting an $O(q^2/a)$ amount from the area, which cannot be included in the area evaluation at $O(1)$.

As can be seen from the inset in Fig. 3, the mean-driven approximation via Eqs. (28) improves with decreasing f near the upper turning point of the gain curve and eventually also along its unstable branch, but is always the least accurate in an $O(\sqrt{f})$ neighborhood of the point $(f\nu,m)=(B-1,0)$. In particular, recall that in the zero-fluctuations limit discussed in Sec. V, this point separates two very distinct regimes of the probability density function $\rho(v)$: $\rho(v)=\delta(v-V_S)$ along the $f\nu$ axis and $\rho(v)$ given by Eq. (24) along the gain curve parametrized by Eqs. (28), with a discontinuous transition between the two at the threshold point $(f\nu,m)=(B-1,0)$.

IX. VALIDITY OF THE FOKKER-PLANCK DESCRIPTION

In this section, we discuss the accuracy of the gain curves and voltage probability density functions obtained using the Fokker-Planck equation (20) as an approximation to their counterparts in a more realistic IF network with finite rise and decay conductance times obtained via direct numerical simulations. In these simulations, we used an IF model of the same form as Eq. (1), but with the instantaneous δ-function conductance time course replaced by the α-function time course

$$G(t)=\frac{1}{\sigma_d-\sigma_r}[\exp(-t/\sigma_d)-\exp(-t/\sigma_r)]\theta(t), \qquad (52)$$

where $\theta(t)$ is the Heaviside function, i.e., $\theta(t)=1$ for $t>0$ and 0 otherwise. For the δ-function conductance time course assumed in the model (1) to be a good approximation of the more realistic conductance time course (52), short conductance rise and decay times, $\sigma_r=0.1$ ms and $\sigma_d=0.2$ ms, were used in the simulations.

From Secs. II and IV, we recall that the quantity controlling the validity of both the Poisson approximation of the network spike train and the diffusion approximation leading to the Fokker-Planck equation (20) from the kinetic equation (5) is the number of spikes that a neuron at the reset value ε_r must receive in order to spike itself. The requirement that this number must be sufficiently large results in the estimates in Eq. (14), which imply that the strength of the external driving spikes, f, must be small and the effective size of the network, pN, large. To examine how the validity of Eq. (20) deteriorates with f increasing and pN decreasing at the same rate, we compare a set of theoretical gain curves (cf. Fig. 3) with gain curves computed via direct numerical simulations at the same parameter values. The results are presented in Fig. 8.

We remark that, as the strength of the external driving spikes, f, decreases and the effective size of the network, pN, increases, the simulated IF network develops a strong tendency to oscillate in a nearly synchronized, periodic manner [67,73,74]. Because of this tendency, the basin of attraction of the steady asynchronous solution studied here, described by the probability density function $\rho(v)$, becomes exceedingly small for small f and large pN. This leads to the difficulty of observing this solution in simulations even for very small synaptic release probability. The tendency of the network to oscillate can be broken by incorporating into the model additional physiological effects, such as random transmission delays which are due to randomness in axonal propagation velocities and lengths [75–77]. These delays do not alter the *steady-state* equation (23) or its solution $\rho(v)$

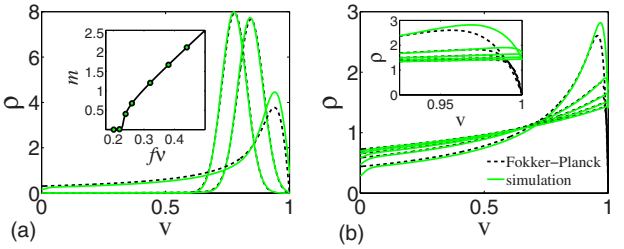

FIG. 9. (Color online) Voltage probability density functions obtained via the Fokker-Planck equation (20) and numerical simulations for the external driving spike strength $f=0.002$ and the effective network size $pN=500$, for which Eq. (20) gives a valid approximation. Starting with the graph with the highest maximum and ending with the graph with the lowest maximum, the corresponding values of the external driving $f\nu$ are (a) 0.2, 0.22, 0.24, (b) 0.26, 0.32, 0.38, 0.44, and 0.5. Other parameter values are $\tau=1$, $S=0.1$, and $\delta_s=0.0002$. The reversal and threshold potentials satisfy Eq. (2). The minimal number of spike-induced voltage jumps needed for a neuron to reach V_T beginning at ε_r, computed from Eq. (14), is ~ 100. In the simulations, $N=10^4$ and $p=0.05$. Poisson-distributed random delays were used in the simulation; the average delay was 4 ms. Inset (a): the locations of the displayed voltage probability density functions along the gain curve. The value of the probability density function's maximum decreases with increasing value of $f\nu$ along the gain curve. Inset (b): the probability density functions obtained via simulations do not satisfy the boundary condition (10) due to finite rise and decay conductance times.

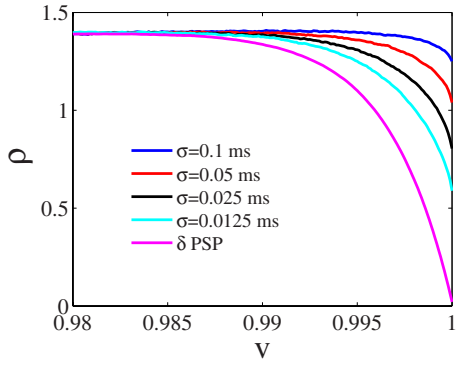

FIG. 10. (Color online) Detail near $v=V_T$ of the voltage probability density computed via numerical simulations for a feedforward neuron with the external driving spike strength $f=0.0025$ and the driving strength $f\nu=40$. Other parameter values are $\tau=1(=20$ ms), $S=0$, and $N=1$. The reversal and threshold potentials satisfy Eq. (2). The conductance rise time in Eq. (52) is instantaneous, $\sigma_r=0$. The decay conductance time $\sigma=\sigma_d$ is varied as shown in the legend, with δ-PSP denoting the instantaneous conductance time course used in Eq. (1). Note how the value of $\rho(V_T)$ decreases with decreasing σ_d and vanishes for δ-PSP.

[67]. We incorporated Poisson-distributed delays in the IF neuronal network simulation to obtain the gain curve for $f=0.002$ in Fig. 8 and the corresponding probability density functions $\rho(v)$, as shown in Fig. 9.

For the external driving spike strength $f=0.002$ (and the corresponding effective network size $pN=500$), we can see that the agreement between the theoretically and numerically obtained gain curves in Fig. 8 is excellent. For these values of f and N, the minimal number of spike-induced jumps that a neuron with the reset membrane-potential value must receive in order to spike itself equals ~ 100. In Fig. 9, we show a comparison between the theoretical voltage probability density functions and those obtained via numerical simulation for the same value set of the external-drive strength $f\nu$. We see that the agreement is generally very good, except, for the probability density functions in the mean-driven regime, near the reset value at $v=\varepsilon_r$ and the threshold value $v=V_T$. These two regions of discrepancy arise due to a common reason, which is because the vanishing boundary condition $\rho(V_T)=0$ in Eq. (10) is not satisfied. This is a consequence of the finite (rise and) decay conductance time(s), as explicitly demonstrated in Fig. 10. We will elaborate more on this point in the discussion in Sec. X.

The two leftmost pairs of gain curves in Fig. 8 correspond to the larger values of the external driving spike strength, $f=0.1$ and 0.025, and the proportionally smaller values of the effective network sizes, $pN=10$ and 40. For these values of f and pN, the minimal numbers of spike-induced voltage jumps needed to reach threshold are 2 and 8, respectively. From Fig. 8, we see that the theoretically and numerically obtained gain curves still agree quite well for low values of the driving $f\nu$ when the firing rates are also low. In particular, the theoretical gain curves can be used to predict quite well when the firing rates will start increasing and their sizes will become $O(1)$. However, the theoretical curves cannot be used to predict correctly the straight-line asymptotes of the numerically obtained gain curves because the theoretically predicted slopes are too large. In particular, the straight-line asymptotes of the numerically obtained gain curves all seem to converge to the straight-line asymptote of the mean-driven gain curve corresponding to the same parameter values, in contrast to those of the theoretically predicted gain curves. This discrepancy clearly signifies the breakdown of the validity of the Fokker-Planck equation (20) in the large f, small pN regime.

To shed further light on how the validity of the Fokker-Planck equation (20) breaks down with increasing external driving spike strength f and decreasing effective network size pN, we display in Fig. 11 the contrast between the voltage probability density functions $\rho(v)$ computed via the Fokker-Planck equation (20) and numerical simulations for the external driving spike strength $f=0.1$ and effective network size $pN=10$. For this spike strength and network size, the diffusion approximation leading to the Fokker-Planck equation (20) is clearly invalid, as only two consecutive external driving spikes suffice to propel a network neuron to fire. One can see from Fig. 11 that the two sets of functions $\rho(v)$ still share some amount of similarity, e.g., their means progressively move toward higher membrane-potential values with increasing external driving strength $f\nu$. On the other hand, the details of the two density sets are very different, with the numerically obtained densities being much rougher.

Finally, we discuss the implications of the theoretically predicted bistability. This bistability underlies the hysteresis that can be observed in the simulations. By slowly ramping the strength $f\nu$ of the external drive up and down through the bistability interval [26], the resulting network firing rate

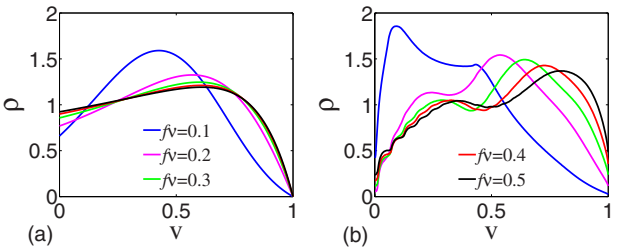

FIG. 11. (Color online) Voltage probability density (a) obtained theoretically from the Fokker-Planck equation (20) and (b) computed via numerical simulations for the fixed external driving spike strength $f=0.1$ and the effective network size $pN=10$, for which Eq. (20) is not a valid approximation. Other parameter values are $\tau=1$, $S=0.1$, and $\delta_s=0.0002$. The reversal and threshold potentials satisfy Eq. (2). The values of the external driving strength $f\nu$ increase from the graphs with the highest to the graphs with the lowest maxima. In the simulations, $N=10^4$ and $p=0.001$. The minimal number of spike-induced voltage jumps needed for a neuron to reach V_T beginning at ε_r, computed from Eq. (14), is ~ 2.

traces out the bottom and top stable branches of the gain curve, respectively, and undergoes sharp jumps to the remaining stable branch near the saddle-node bifurcation points where one stable branch disappears. The size of the hysteresis loops depends on the ramping speed. The slower the ramping speed, the closer are the loops to the theoretically predicted bistability curves. Examples of such hysteresis loops for the small-fluctuation regime are presented in Fig. 12 and show good agreement between the theoretical gain-curve prediction and the hysteretic gain curve branches computed via numerical simulations. On the left, the result of a simulation with a very slow ramping speed is shown. On the right, the results of 50 simulations with a faster ramping speed show that, at faster speeds, jumps are initiated at random $f\nu$ values in the vicinity of the bifurcation values. Moreover, the resulting hysteresis loops are smaller than for the slower ramping speed. Note that, in the mean-driven limit ($f\to 0$, $N\to\infty$, $\nu\to\infty$, $f\nu$ finite), the jump on the up-ramp branch would be initiated near the point $f\nu=B-1$, $m=0$. We should remark that the probability of fluctuation-induced random transitions between the two stable branches is very small in our small-fluctuation regime and we have not observed them in our simulations. Moreover, due to random transmission delays incorporated in our system, the asynchronous regime becomes more stable. We have thus not yet observed switching between the asynchronous and fast oscillatory regimes, which were reported for a discrete model without leakage in [74].

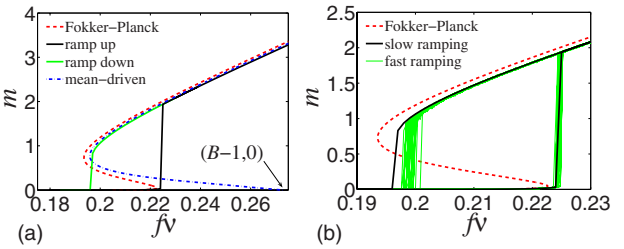

FIG. 12. (Color online) (a) Bistability and hysteresis in gain curves obtained theoretically from the Fokker-Planck equation (20) and the mean-driven approximation (28) and computed via numerical simulations for the external driving spike strength $f=0.002$ and the effective network size $pN=500$. Note that the mean-driven theory would predict the jump on the up-ramp branch of the gain curve obtained by the simulations to be initiated near the point $f\nu=B-1$, $m=0$. Other parameter values are $\tau=1$, $S=0.2$, and $\delta_s=0.0002$. The reversal and threshold potentials satisfy Eq. (2). In the simulations, $N=10^4$ and $p=0.05$. For each value of $f\nu$, $\tau_{f\nu}=10$ s of the network evolution was simulated. The difference between two consecutive $f\nu$ values was $\Delta(f\nu)=0.001$, giving the speed 10^{-4} s^{-1}. Poisson-distributed random transmission delays averaging 4 ms were used. (b) Hysteresis obtained in the simulations using fast and slow ramping speeds. The hysteretic gain-curve branches obtained for the slow ramping speed are the same as on the top. For the gain curves obtained by fast ramping, an ensemble of 50 simulation results is shown, with $N=10^3$, $p=0.5$, $\tau_{f\nu}=1$ s, $\Delta(f\nu)=0.0004$, and speed$=4\times 10^{-4}$ s^{-1}.

X. DISCUSSION

In this work, we have addressed the basic properties of the Fokker-Planck equation describing the conductance-based IF neuronal network model. In addition to the assumption that the dynamics of a neuronal network can be adequately captured by one-point statistics, three main assumptions lead to the description using the Fokker-Planck equation. The first is the vanishing of the conductance rise and decay time scales. The second is that the network dynamics is asynchronous, and the spike times of the entire network can be approximated by a Poisson train. The third is the diffusion approximation, justified when each neuron receives large numbers of spikes, each inducing only a very small change of this neuron's membrane potential, which appears to be the case in some cortical neurons *in vivo* [78].

We have addressed the consequences of the above second and third assumptions in Sec. IX. In particular, we showed that the gain curves and probability density functions obtained via the Fokker-Planck equation (20) closely match those obtained using numerical simulations of an IF network with short but finite conductance rise and decay times in the regime of small synaptic-input fluctuations in which the two assumptions are valid. We also described how this comparison deteriorates with increasing amounts of synaptic-input fluctuations.

We should remark that we avoided numerical simulations with the instantaneous conductance time scale and the related question of whether and how the solutions of the Fokker-Planck equation (20) and the corresponding solutions of the kinetic equation (5) converge to one another in the limit as the strength of the external-drive spikes f vanishes and the Poisson rate ν of the external drive and the network size N increase without a bound. This question is nontrivial in particular because Eq. (20) is not the corresponding asymptotic limit of Eq. (5); instead, it is the second-order truncation for f small and ν and N large but finite in the Kramers-Moyal expansion of Eq. (5) [27]. In the time-independent case, the true asymptotic limit is the mean-driven equation (24), which is equivalent to the first-order truncation of Eq. (5) and is thus a highly singular limit. The

likely complicated nature of the approach to this limit can be gleaned from the highly oscillatory behavior of the voltage probability density function, described by an equation analogous to Eq. (5), even for a *feed-forward*, current-based IF neuron [79]. Therefore, studying this limit will be relegated to a future publication.

The assumption of asynchronous dynamics becomes violated for small values of the input fluctuations when the network exhibits synchronous oscillations. As was seen in Sec. IX, in this case, decreasing the synaptic release rate and/or including random transmission delays [75–77] help to stabilize the asynchronous solutions, thus giving rise to the corresponding gain curves described here. Oscillations in a current-driven IF model analogous to Eq. (1), with a time-periodically modulated Poisson rate of the external drive, were studied in [46,53,80]. In our recent study [67] of synchrony in the current-driven version of the IF model (1), the asynchronous solutions of the current-driven IF model and the bistability of its gain curves were similarly addressed using random transmission delays.

Incorporation of finite conductance rise and decay times changes the kinetic theory approach dramatically. In particular, Eqs. (5) and (20) in this case become partial differential (-difference) equations with time, voltage, and conductance(s) as independent variables and an additional closure needs to be employed to address the voltage statistics alone [54,55]. After the diffusion approximation leading to the analog of Eq. (20) is made, this closure is obtained via the maximal entropy principle [56]. The resulting kinetic theory consists of a system of equations, which in the simplest scenario describe the voltage probability density and the first conductance moment conditioned on the voltage value. The Fokker-Planck equation (20) can be recovered from this system in the limit of vanishing conductance time scales when the conditional conductance moment becomes slaved to the voltage probability density $\rho(v)$. However, while the periodic flux boundary condition (21) is retained in this description, the absorbing boundary condition (10) is replaced by a periodic boundary condition for the conditional conductance moment, i.e., the condition $(V_T-\varepsilon_E)\rho(V_T)=(\varepsilon_r-\varepsilon_E)\rho(\varepsilon_r)$. The difference in the boundary conditions stems from the noncommuting of two different limits: vanishing fluctuations and vanishing conductance time scales. The Fokker-Planck descriptions with the two differing boundary conditions produce very similar results [55], except for the values of $\rho(v)$ very close to the firing threshold $v=V_T$. Note that the probability density functions in Fig. 9, in particular, in its inset, further demonstrate this point. (See also the corresponding discussion in Sec. IX.) Therefore, both sets of boundary conditions can be useful, but the conditions for the use of either should depend on the physiological modeling requirements in each specific case under investigation.

Finally, we remark that while this paper addresses asynchronous dynamics of an idealized neuronal network model, the underlying bifurcation scenario of the gain curves, which are bistable in the regime of small synaptic-input fluctuations and become single-valued as the amount of synaptic-input fluctuations increases, remains valid in much more realistic neuronal models. In particular, similar bistability is present in the gain curves of excitatory complex cells in models of orientation and spatial-frequency tuning in the primary visual cortex, which cover four orientation pinwheels with $\sim 10^4$ neurons, with both excitatory and inhibitory as well as simple and complex cells, and incorporate realistic cortical architecture [26,81]. In these models, the amount of fluctuations is controlled by the sparsity of synaptic connections and/or the ratio between the amounts of fast and slow excitatory conductances. The knowledge of the underlying bifurcation structure makes it possible to constrain the model parameters, in particular, the amount of sparsity, so that the models operate in physiologically plausible regimes and reproduce the correct properties of the tuning curves [26,81]. This bifurcation scenario was therefore in these modeling works a crucial element in the understanding of the mechanisms that produce the correct tuning curves in the computational models of the primary visual cortex.

ACKNOWLEDGMENTS

A.V.R. and D.C. were partly supported by NSF under Grants No. DMS-0506396 and No. DMS-0507901 and a grant from the Swartz Foundation. L.T. was supported by the NSF under Grant No. DMS-0506257. G.K. was supported by NSF under Grant DMS-0506287 and gratefully acknowledges the hospitality of New York University's Courant Institute of Mathematical Sciences and Center for Neural Science.

APPENDIX: UNIFORM ASYMPTOTICS FOR THE VOLTAGE PROBABILITY DENSITY

In this appendix, we present a derivation of the asymptotic formula (40) for the probability density function $\varrho(x)$, which was used in Sec. VII. For this purpose, we use the result of [71] concerning asymptotic behavior of the complementary incomplete γ function, defined by

$$\Gamma(\alpha,z)=\int_z^\infty t^{\alpha-1}e^{-t}dt \tag{A1}$$

for α, $z>0$, and by analytic continuation elsewhere. Defining

$$\eta=\mathrm{sgn}\left(\frac{z}{\alpha}-1\right)\sqrt{\frac{z}{\alpha}-1-\ln\frac{z}{\alpha}} \tag{A2}$$

for $z/\alpha>0$ and by analytic continuation elsewhere, [71] states that the asymptotic expansion

$$e^{-i\pi\alpha}\Gamma(-\alpha,ze^{-\pi i})\sim\frac{1}{\Gamma(\alpha+1)}\left[\pi i\,\mathrm{erfc}\left(-i\eta\sqrt{\frac{\alpha}{2}}\right)+\sqrt{\frac{2\pi}{\alpha}}e^{\alpha\eta^2/2}\left(\frac{1}{\eta}-\frac{1}{z/\alpha-1}\right)\right]+O(e^{\alpha\eta^2/2}\alpha^{-3/2}), \tag{A3}$$

holds for the complementary incomplete gamma function (A1) uniformly as $\alpha\to\infty$ and $|\arg z|<\pi-\delta$, for any small δ. Here, $\mathrm{erfc}(\cdot)$ is the complementary error function $\mathrm{erfc}(z)=(2/\sqrt{\pi})\int_z^\infty e^{-t^2}dt$. We remark that as $z\to\alpha$, the apparent sin-

gularity in Eq. (A3) cancels out because $1/\eta - 1/(z/\alpha - 1) \to 1/3$.

We are interested in the asymptotic expansion of the probability density $\varrho(x)$ in Eq. (35) for small values of q^2/a, which is uniform in x, a, and q, in particular around the transition point $a=B$. The key to this expansion is the corresponding asymptotic expansion of the integral in Eq. (35),

$$F(x) = \int_x^B s^{-a/q^2-1} e^{s/q^2} ds. \tag{A4}$$

Using the substitution $s=q^2 v e^{i\pi}$, Eq. (A4) can be rewritten in the form

$$F(x) = q^{-2a/q^2} e^{-i\pi a/q^2} \left[\Gamma\left(-\frac{a}{q^2}, \frac{x}{q^2} e^{-i\pi}\right) - \Gamma\left(-\frac{a}{q^2}, \frac{B}{q^2} e^{-i\pi}\right) \right], \tag{A5}$$

where $\Gamma(\cdot,\cdot)$ is again the complementary incomplete gamma function (A1). Thus, in our problem, $z=x/q^2$ and $\alpha=a/q^2$, and we can again put $\eta=\eta(x)$ as in Eq. (A2). Equations (A3) and (A5), and Stirling's formula for $\Gamma(a/q^2+1)$, then give the two-term expansion

$$\begin{aligned} F(x) \sim \frac{q}{\sqrt{2\pi}} a^{-a/q^2+1/2} e^{a/q^2} \Bigg[& i\pi \operatorname{erfc}\left(-\frac{i\eta(x)}{q}\sqrt{\frac{a}{2}}\right) \\ & - \sqrt{\frac{2\pi}{a}} q e^{a\eta^2(x)/2q^2} \left(\frac{1}{x/a-1} - \frac{1}{\eta(x)}\right) \\ & - i\pi \operatorname{erfc}\left(-\frac{i\eta(B)}{q}\sqrt{\frac{a}{2}}\right) \\ & + \sqrt{\frac{2\pi}{a}} q e^{a\eta^2(B)/2q^2} \left(\frac{1}{B/a-1} - \frac{1}{\eta(B)}\right) \Bigg]. \end{aligned} \tag{A6}$$

From Eqs. (35), (A4), and (A6) and the formula $\operatorname{erfc}(-iz) = 1 + 2iD(z)/\sqrt{\pi}$, with $D(z)$ being the Dawson integral (42), we finally obtain the expansion (40).

We remark that the simplified expansions (45) and (51) can easily be obtained from Eq. (40) using the large-z asymptotic behavior of the Dawson integral, $D(z) \sim 1/2z + O(1/z^3)$.

Numerically, the expansion (40) was evaluated as follows. The Dawson integral (42) was computed using its piecewise-smooth approximation by rational functions and continued fractions with eight terms, developed in [82]. The difference $1/\eta(x) - 1/(x/a-1)$ was computed exactly for $|x-a| \geq \delta_0$ and using a ten-term Taylor-series expansion around $x=a$ for $|x-a| \leq \delta_0$, with $\delta_0 = 10^{-2}$.

[1] L. Boltzmann, Wien. Ber. **58**, 517 (1868); reprinted in *Abhandlungen*, Vol. 1 (Barth, Leipzig, 1909), p. 49.
[2] L. Boltzmann, Wien. Ber. **66**, 275 (1872); reprinted in *Abhandlungen*, Vol. 1 (Barth, Leipzig, 1909), p. 316.
[3] K. Hasselmann, J. Fluid Mech. **12**, 481 (1962).
[4] K. Hasselmann, J. Fluid Mech. **15**, 273 (1963).
[5] D. Benney and P. Saffman, Proc. R. Soc. London, Ser. A **289**, 301 (1966).
[6] V. E. Zakharov, Sov. Phys. JETP **24**, 740 (1967).
[7] V. E. Zakharov and N. Filonenko, Sov. Phys. Dokl. **11**, 881 (1967).
[8] V. E. Zakharov, J. Appl. Mech. Tech. Phys. **2**, 190 (1968).
[9] D. J. Benney and A. C. Newell, Stud. Appl. Math. **48**, 29 (1969).
[10] H. R. Wilson and J. D. Cowan, Biophys. J. **12**, 1 (1972).
[11] B. Knight, J. Gen. Physiol. **59**, 734 (1972).
[12] A. N. Pushkarev and V. E. Zakharov, Phys. Rev. Lett. **76**, 3320 (1996).
[13] A. Majda, D. McLaughlin, and E. Tabak, J. Nonlinear Sci. **7**, 9 (1997).
[14] D. Cai, A. J. Majda, D. W. McLaughlin, and E. G. Tabak, Proc. Natl. Acad. Sci. U.S.A. **96**, 14216 (1999).
[15] D. Cai, A. J. Majda, D. W. McLaughlin, and E. G. Tabak, Physica D **152-153**, 551 (2001).
[16] A. I. Dyachenko, A. O. Korotkevich, and V. E. Zakharov, Phys. Rev. Lett. **92**, 134501 (2004).
[17] V. E. Zakharov, A. O. Korotkevich, A. Pushkarev, and D. Resio, Phys. Rev. Lett. **99**, 164501 (2007).
[18] D. Somers, S. Nelson, and M. Sur, J. Neurosci. **15**, 5448 (1995).
[19] T. Troyer, A. Krukowski, N. Priebe, and K. Miller, J. Neurosci. **18**, 5908 (1998).
[20] D. McLaughlin, R. Shapley, M. Shelley, and J. Wielaard, Proc. Natl. Acad. Sci. U.S.A. **97**, 8087 (2000).
[21] L. Tao, M. Shelley, D. McLaughlin, and R. Shapley, Proc. Natl. Acad. Sci. U.S.A. **101**, 366 (2004).
[22] D. Cai, A. Rangan, and D. McLaughlin, Proc. Natl. Acad. Sci. U.S.A. **102**, 5868 (2005).
[23] A. V. Rangan, D. Cai, and D. W. McLaughlin, Proc. Natl. Acad. Sci. U.S.A. **102**, 18793 (2005).
[24] R. Brette *et al.*, J. Comput. Neurosci. **23**, 349 (2007).
[25] N. Carnevale and M. Hines, *The NEURON Book* (Cambridge University Press, Cambridge, England, 2006).
[26] L. Tao, D. Cai, D. McLaughlin, M. Shelley, and R. Shapley, Proc. Natl. Acad. Sci. U.S.A. **103**, 12911 (2006).
[27] H. Risken, *The Fokker-Planck Equation: Methods of Solution and Applications* (Springer-Verlag, New York, 1989).
[28] D. Nykamp and D. Tranchina, J. Comput. Neurosci. **8**, 19 (2000).
[29] M. Rudolph and A. Destexhe, Neural Comput. **15**, 2577 (2003).
[30] M. Rudolph and A. Destexhe, Neural Comput. **17**, 2301 (2005).
[31] M. Rudolph and A. Destexhe, Neural Comput. **18**, 2917 (2006).
[32] M. J. E. Richardson, Phys. Rev. E **69**, 051918 (2004).
[33] M. J. E. Richardson and W. Gerstner, Neural Comput. **17**, 923 (2005).

[34] B. Lindner and A. Longtin, Neural Comput. **18**, 1896 (2006).
[35] H. Wilson and J. Cowan, Kybernetik **13**, 55 (1973).
[36] A. Treves, Network **4**, 259 (1993).
[37] R. Ben-Yishai, R. Bar-Or, and H. Sompolinsky, Proc. Natl. Acad. Sci. U.S.A. **92**, 3844 (1995).
[38] M. Shelley and D. McLaughlin, J. Comput. Neurosci. **12**, 97 (2002).
[39] P. C. Bressloff, J. Cowan, M. Golubitsky, P. Thomas, and M. Wiener, Philos. Trans. R. Soc. London., Ser. B **356**, 299 (2001).
[40] W. Wilbur and J. Rinzel, J. Theor. Biol. **105**, 345 (1983).
[41] L. F. Abbott and C. van Vreeswijk, Phys. Rev. E **48**, 1483 (1993).
[42] T. Chawanya, A. Aoyagi, T. Nishikawa, K. Okuda, and Y. Kuramoto, Biol. Cybern. **68**, 483 (1993).
[43] D. J. Amit and N. Brunel, Cereb. Cortex **7**, 237 (1997).
[44] G. Barna, T. Grobler, and P. Erdi, Biol. Cybern. **79**, 309 (1998).
[45] J. Pham, K. Pakdaman, J. Champagnat, and J. Vibert, Neural Networks **11**, 415 (1998).
[46] N. Brunel and V. Hakim, Neural Comput. **11**, 1621 (1999).
[47] W. Gerstner, Neural Comput. **12**, 43 (2000).
[48] A. Omurtag, B. Knight, and L. Sirovich, J. Comput. Neurosci. **8**, 51 (2000).
[49] A. Omurtag, E. Kaplan, B. Knight, and L. Sirovich, Network **11**, 247 (2000).
[50] D. Nykamp and D. Tranchina, Neural Comput. **13**, 511 (2001).
[51] E. Haskell, D. Nykamp, and D. Tranchina, Network Comput. Neural. Syst. **12**, 141 (2001).
[52] A. Casti, A. Omurtag, A. Sornborger, E. Kaplan, B. Knight, J. Victor, and L. Sirovich, Neural Comput. **14**, 957 (2002).
[53] N. Fourcaud and N. Brunel, Neural Comput. **14**, 2057 (2002).
[54] D. Cai, L. Tao, M. Shelley, and D. McLaughlin, Proc. Natl. Acad. Sci. U.S.A. **101**, 7757 (2004).
[55] D. Cai, L. Tao, A. V. Rangan, and D. W. McLaughlin, Commun. Math. Sci. **4**, 97 (2006).
[56] A. V. Rangan and D. Cai, Phys. Rev. Lett. **96**, 178101 (2006).
[57] A. N. Burkitt, Biol. Cybern. **95**, 1 (2006).
[58] S. Redman, Physiol. Rev. **70**, 165 (1990).
[59] N. Otmakhov, A. M. Shirke, and R. Malinow, Neuron **10**, 1101 (1993).
[60] C. Allen and C. F. Stevens, Proc. Natl. Acad. Sci. U.S.A. **91**, 10380 (1994).
[61] N. R. Hardingham and A. U. Larkman, J. Physiol. (London) **507**, 249 (1998).
[62] S. J. Pyott and C. Rosenmund, J. Physiol. (London) **539**, 523 (2002).
[63] M. Volgushev, I. Kudryashov, M. Chistiakova, M. Mukovski, J. Niesmann, and U. T. Eysel, J. Neurophysiol. **92**, 212 (2004).
[64] E. Cinlar, in *Stochastic Point Processes: Statistical Analysis, Theory, and Applications*, edited by P. Lewis (Wiley, New York, 1972), pp. 549–606.
[65] M. Shelley, D. McLaughlin, R. Shapley, and J. Wielaard, J. Comput. Neurosci. **13**, 93 (2002).
[66] Y. Kuramoto, Physica D **50**, 15 (1991).
[67] K. A. Newhall, G. Kovačič, P. R. Kramer, D. Zhou, A. V. Rangan, and D. Cai, Comm. Math. Sci. (to be published).
[68] L. J. Slater, *Confluent Hypergeometric Functions* (Cambridge University Press, New York, 1960).
[69] L. J. Slater, *Generalized Hypergeometric Functions* (Cambridge University Press, Cambridge, England, 1966).
[70] K. E. Muller, Numer. Math. **90**, 179 (2001).
[71] N. M. Temme, Methods Appl. Anal. **3**, 335 (1996).
[72] F. W. J. Olver, *Asymptotics and Special Functions*, AKP Classics (A K Peters Ltd., Wellesley, MA, 1997).
[73] R. E. Mirollo and S. H. Strogatz, SIAM J. Appl. Math. **50**, 1645 (1990).
[74] R. E. L. DeVille and C. S. Peskin, Bull. Math. Biol. **70**, 1608 (2008).
[75] P. L. Nunez, *Neocortical Dynamics and Human EEG Rhythms* (Oxford University Press, New York, 1995).
[76] V. Bringuier, F. Chavane, L. Glaeser, and Y. Fregnac, Science **283**, 695 (1999).
[77] R. Eckhorn, A. M. Gail, A. Bruns, A. Gabriel, B. Al-Shaikhli, and M. Saam, IEEE Trans. Neural Netw. **15**, 1039 (2004).
[78] D. Pare, E. Shink, H. Gaudreau, A. Destexhe, and E. Lang, J. Neurophysiol. **79**, 1450 (1998).
[79] L. Sirovich, A. Omurtag, and B. W. Knight, SIAM J. Appl. Math. **60**, 2009 (2000).
[80] N. Brunel, J. Comput. Neurosci. **8**, 183 (2000).
[81] W. Zhu, M. Shelley, and R. Shapley, J. Comput. Neurosci. **26**, 271 (2009).
[82] W. J. Cody, K. A. Paciorek, and H. C. Thacher, Jr., Math. Comput. **24**, 171 (1970).